Received: 29 January 2024 | Accepted: 3 March 2024

DOI: 10.1049/rsn2.12557

IET Radar, Sonar & Navigation

The Institution of Engineering and Technology WILEY

ORIGINAL RESEARCH

Time transfer via single-record TDoA measurements of GNSS satellites using direct cross-correlation and relative pilot code phases

Erik Busley | **Timotej Žuntar** | **Jörg Borgmann** | **Michael Krist**

Fraunhofer Institute for High Frequency Physics and Radar Techniques FHR, Wachtberg, Germany

Correspondence

Erik Busley.
Email: Erik.Busley@FHR.Fraunhofer.de

Funding information

Deutsches Zentrum für Luft- und Raumfahrt, Grant/Award Number: 50LZ2001

Abstract

Radar systems are evolving towards distributed receiver networks. As individual stations might be separated too far to install a cable link, novel methods are required to synchronise individual data records in the time domain. State-of-the-art GNSS receivers disciplining a highly stable oscillator are able to output a timing signal with several nanosecond accuracy solely using non-proprietary signals. However, they typically require a stable environment and become a major cost factor for receiver networks with a high number of nodes. A method is presented to passively synchronise data records via GNSS raw signals in a single record requiring only a GNSS antenna, an analogue-to-digital converter and computation hardware. The clock bias is estimated via the common view method with either full raw signal correlation or software-based code correlation of individual signals from the GPS, Galileo and BeiDou constellation with sub-nanosecond precision.

KEYWORDS

atomic clocks, binary sequences, correlation methods, cost reduction, delay estimation, global positioning system, multistatic radar, synchronisation

1 | INTRODUCTION

Data synchronisation is a major issue in distributed sensor networks when each site operates on its own independent timescale. The stability requirements are especially high in radar networks, particularly in networks utilising coherent data fusion methods [1]. Although modern clocks that infer local time from global navigation satellite systems (GNSS) offer timing on the nanosecond level and are routinely employed in radar nodes [1, 2], those devices can become a significant cost factor in extended networks. Moreover, small aerial vehicles are gaining significance as radar platforms [3], often with severe weight limitations or operating in environments not suited to host a stable oscillator. Typically, the importance of accurately tracking an absolute timescale (e.g. UTC) is less significant than that of minimising relative time and frequency offsets between the nodes. In this work, we present a simple-to-use method for sub-nanosecond synchronisation of data record by simultaneous recording of raw GNSS signals that achieves high precision even on the single-record level. A necessary requirement is a high performance analogue to digital converter which, however, is present in many radar systems. In some cases, for example, phased array systems for space surveillance [4], the primary antenna could potentially be used for data collection if operating in the correct frequency band.

Unlike sophisticated algorithms implemented in high-end commercial GNSS-based clocks, the presented method has its focus on simplicity. In recent years, modernised GNSS signals with higher power and improved correlation properties combined with advances in desktop computer speed allow for a custom analysis of GNSS raw data. Post-processing of the raw signal in a local software environment renders this method independent of any external services providing real time corrections as well as resilient to some error sources.

2 | SYNCHRONISATION METHOD

For synchronisation we employ a method known as common view [5] in its multi-channel, multi-constellation version; Figure 1 illustrates the working principle. To estimate the inter-site clock bias at a given time, one or multiple recordings are made at each site within a time interval over which the clock bias can be considered nearly constant and correlated with local signal copies of all satellites in common view. The instantaneous clock bias $\tau_{\text{clock}}(t)$ is then determined by a weighted average of single-differenced correlation delays. The precision of the method can be estimated using the statistic of double differences. Sampling the signal at a frequency comparable to GNSS carrier frequency enables correlation with higher precision than achievable by baseband correlators and bridges the gap between code and carrier phase [6] or interferometric observations [7].

Consider a satellite signal sent from position $\boldsymbol{x}_{\text{sat}}$ and received by two stations at positions $\boldsymbol{x}_{1,2}$, then the unbiased time difference of arrival (TDoA) reads.

$$\text{TDoA}(t) = (\|\boldsymbol{x}_{\text{sat}}(t) - \boldsymbol{x}_1\| - \|\boldsymbol{x}_{\text{sat}}(t) - \boldsymbol{x}_2\|)/c \quad (1)$$

$$= \text{TDoA}_{\text{obs}}(t) - \tau_{\text{clock}}(t) - \epsilon(t) \quad (2)$$

Where $\|\cdot\|$ is the Euclidean norm and c is the speed of light. If $\boldsymbol{x}_{\text{sat}}(t)$ is known, the difference between observed TDoA $\text{TDoA}_{\text{obs}}(t)$ and its prediction are the clock bias $\tau_{\text{clock}}(t)$ plus an offset term $\epsilon(t)$ arising from for example, different cable lengths or varying antenna phase centres as a function of frequency and incidence angle. As $\epsilon(t)$ is nearly constant for a given setup and hence acts as an offset of the clock bias measurement it is disregarded in later discussions.

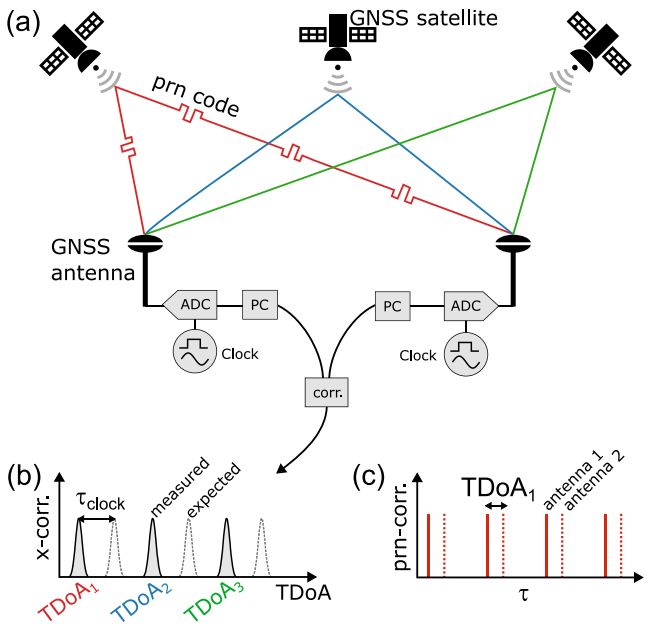

FIGURE 1 Clock offset measurement via multi-channel common view. (a) GNSS satellites encode data in periodic pseudo random noise (PRN) chips. Data records are saved on a computer for further data processing. (b) When the signal of two antennas is cross-correlated, each satellite causes a correlation peak at a predictable time delay TDoA_i. The clock offset τ_{clock} is determined by cross-correlation of both signals and comparison of the signal with its prediction. (c) Estimation of τ_{clock} by correlating PRN code chips in each signal and comparing their measured TDoA with its prediction.

2.1 | GNSS signal structure

Except for legacy GLONASS signals, all active GNSS constellations use code division multiple access (CDMA) techniques to distinguish between signals from different satellites in the same frequency band; all satellites continuously transmit at the same frequency, but their data transmissions are modulated by pseudo-random binary sequences (primary codes) which ensure near total orthogonality, and autocorrelation properties for some newer signals are further improved with the use of subcarrier modulation and secondary codes [6]. The signals are transmitted on different carrier frequencies ranging from f_c = 1176.45–1575.42 MHz and modulated by phase shift keying with f_{mod} = 1.023–10.23 MHz, even though the actual symbol transmission rate does not surpass 1 kHz. In general, a given signal consists of multiple components with different repetition periods; the primary code (shortest period, t_r = 1–20 ms) is repeated an integer number of times within each transmitted symbol.

3 | EXPERIMENTAL SETUP

For GNSS signal reception, we employ a pair of commercial multi frequency GNSS survey antennas (SparkFun SPK6618H) with a frequency-dependent directional gain of 2.5 dBi to 5 dBi (38 ± 2) dB active LNA gain and a noise figure of max. 1.8 dB. The antennas are connected to an analogue-digital-converter (ADC) that directly samples the signal at a frequency of f_s = 3250 MHz, with no intermediate mixing stage being used (digitiser model: SP Devices ADQ36). The signal damping between antenna and ADC is estimated to be < 10 dB. The internal clocks of the ADCs are referenced with external 10 MHz sinusoids generated by local stable oscillators. The local oscillator for one of the ADCs is a highly stable caesium clock (Axtal AXCS9000HP) whose signal is assumed to be stable and exhibit at most linear drift over the course of a measurement series whereas the second receiver system employs a GNSS-referenced rubidium clock (Safran LNRCLOK-1500). Recordings are triggered by the respective clock's pulse per second (PPS) signal, transferred and saved in binary format for later analysis on a separate computer. The ADCs also provide the time delay between trigger pulse detection and the start of data acquisition with a resolution of 20 ps, which was taken into account to achieve subsample resolution. The stabilities of both clocks far exceed the value required for synchronisation with a single recording. However, this allows for a proper characterisation of the precision. For evaluation of method performance

in the presence of instabilities, the rubidium clock was at times intentionally perturbed to induce a strong clock drift.

Bias voltages for the antenna LNAs were provided by diplexer modules. The digitisers and raw data handling are controlled through a LabView-based interface, while Python was used for data analysis, see Section 4. Satellite positions were calculated from publicly available two-line element (TLE) sets. In the short baseline approximation, signal path distortions like atmospheric and ionospheric refraction cancel out in the TDoA as apparent satellite elevation and speed of light reduction compensate each other. Orbit inaccuracies arising from limited TLE precision cause negligible picosecond-level TDoA biases. For baselines longer than several kilometres, ultra-rapid ephemeris solutions provided by analysis centres of the International GNSS Service and appropriate compensation of environmental factors can be used to ensure maximum accuracy.

Data were recorded employing two experimental configurations: in the first case, the two antennas were set up on a rooftop at the Fraunhofer FHR site in Wachtberg, Germany, at a distance of 25 m and connected to separate channels of the same ADC; in the second, one of the antennas remained at the initial position, while the second antenna, ADC and clock were set up at a distance of 2.36 km to the site. The short baseline approximation is valid in both cases; the geometry of the latter is shown in Figure 2. Every individual record included 50 ms of signal, equivalent to 162.5×10^6 data points per antenna. The time between adjacent recordings was chosen between 10 and 300 s for different datasets due to constraints in necessary storage size and processing time.

In the two-clock configuration, the rubidium clock bias was additionally estimated by a separate GNSS receiver (Septentrio PolaRx5TR) connected to the same secondary antenna as the receiver of the clock and receiving a copy of the clock's 10 MHz signal. The device logs the estimated bias between its internal time and the clock output, which can be used as a further point of comparison. The antenna positions were determined using the mentioned GNSS receiver.

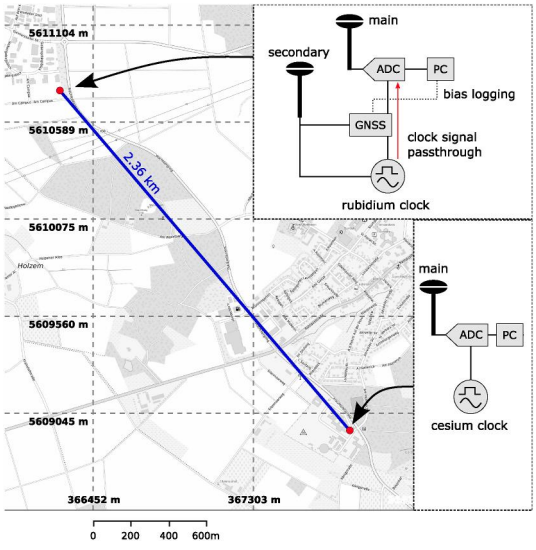

FIGURE 2 Map of the Wachtberg (Germany) area with an illustration of the longer of two antenna site and baseline combinations from which experimental data were gathered as well as the hardware configuration schematic at each site. East and North coordinates are given in UTM system. Geographic data adapted from ref. [8].

Although the ultimate goal of the experiment is measurement of time difference in the PPS signal edges of two different systems, other differences in hardware (e.g. the trigger time resolution or LNA gain) can introduce additional biases which can affect the accuracy of the method even when clock behaviour is precisely known. Therefore, the measurements with a common ADC were necessary to observe the method's precision under optimal conditions, for which we expect a constant time difference.

3.1 | Code generation

For correlation with recordings, synthetic versions of the following GNSS signals were generated: L1C, L5, E1, E5A, E5B, E6, B1C, B1I, B2A, and B3I. We found those signals to contribute the most as compared to for example, L1C/A, L2C/M or L2C/L which have lower bandwidth or the current internal state of overlay shift register needs to be known for proper usage. Pseudo-random primary and secondary code sequences for each sequence number were constructed as specified in, or copied from, interface control documents for GPS [9, 10], Galileo [11] and BeiDou [12] constellations. Depending on the signal, primary sequences can be constructed either from Legendre sequences or the output of linear feedback shift registers with appropriately set initial states and various combinations of time shifts and Boolean operations. Secondary codes are usually explicitly given in the design documents.

Once generated, the components were used to modulate the carrier sinusoid by binary phase shift keying. Since the transmitted data and the relative place in secondary codes are unknown and do not need to be decoded for our approach, only the shortest repeating period of the dataless, pilot components, needed to be generated. This also makes the method immune to any satellite-side data errors, whether accidental or intentional. The signals were synthesised with the same sampling frequency as was used in the recordings, taking into account the predicted Doppler shift. To save computational resources, we only consider satellites above 30° elevation, typically leaving 3 or 4 satellites per constellation. Their orbits are calculated using two-line element (TLE) files obtained from CelesTrak [13] and analysed by an SGP4/SDP4 propagator implemented in Python's Skyfield package [14].

4 | RESULTS

We present two distinct analysis methods: first, cross-correlation of raw signals, followed by cross-referencing and comparison of the observed peak positions with those expected for each satellite as presented in Section 4.1; second,

cross-correlation of bandpass-filtered raw signals with synthesised PRN signals of individual satellites with followed by processing of their arrival times, as presented in Section 4.2. The former method is computationally cheap but requires entire recordings to be transmitted between nodes and is more susceptible to interference. The latter method is more robust and keeps data transfer to a minimum, but requires a large amount of computational resources.

In both cases, the data is analysed using the Python programming language, mostly based on the Numpy package [15] in combination with the Intel® Math Kernel Library for higher performance where possible.

4.1 | Raw correlation

The TDoA of multiple GNSS satellites can be determined simultaneously by cross-correlating (x-corr.) the raw signals. First, the signal is digitally filtered with a frequency response consisting of multiple narrow pass bands around the major GNSS bands, see Figure 3. We find that even weak interferences like the spectral line at 1280 MHz can heavily disrupt the results, which is why an additional notch filter was introduced. Unknown interferences occurring during a measurement series can produce heavy outliers in the results if not handled properly.

The cross-correlation coefficient R_{12} of the zero-mean signals $y_{1,2}$ with $\langle y_i \rangle = 0$ is calculated as follows:

$$R_{12}(\tau) = \frac{(y_1 * y_2)(\tau)}{\sigma_1 \sigma_2} \tag{3}$$

where * is the convolution operator and σ_i are the standard deviations of y_i. The computed correlation signal is reduced to its envelope function via a Hilbert transform and its absolute value is shown in Figure 4a where the grey dashed lines show the predicted unbiased peak positions TDoA_i as calculated from Equation (1). To determine the clock bias, $|R_{12}|$ is correlated once more with the expected peak position signal (a sum of unit impulse functions δ at N expected peak locations),

$$R'_{12}(\tau_{\mathrm{clock}}) = \left(|R_{12}(\tau)| * \sum_{i=1}^{N} \delta(\tau - \mathrm{TDoA}_i) \right)(\tau_{\mathrm{clock}}) \tag{4}$$

yielding the clock bias likelihood, see Figure 4b. The exact position of the maximum is determined by fitting a parabola on the nearest 10 points to either side. In the shown example, this reveals the most likely clock delay of $\tau_{\mathrm{clock}} \approx -83$ ns. When shifted accordingly, the expected correlation peak positions (red) in panel (a) visibly coincide with the correlation peaks. The results of successive measurements are shown in Figure 6 and discussed in Section 5 along with outliers and an estimation of the measurement uncertainty.

In order to accurately determine the clock bias, the direct cross-correlation method requires as many well resolved correlation peaks as possible. Interference of overlapping peaks renders this method unfeasible and puts an effective lower bound on the baseline length, since the peak widths of legacy low-bandwidth signals can approach the 1 microsecond mark.

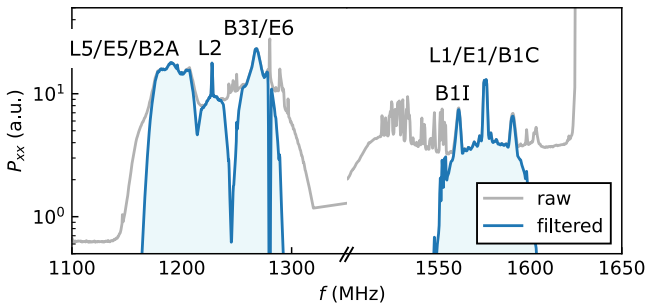

FIGURE 3 Power spectrum of the recorded signals, before and after digital filtering. The raw signal shape represents the pass band of the antenna. Some of the major GNSS bands are marked.

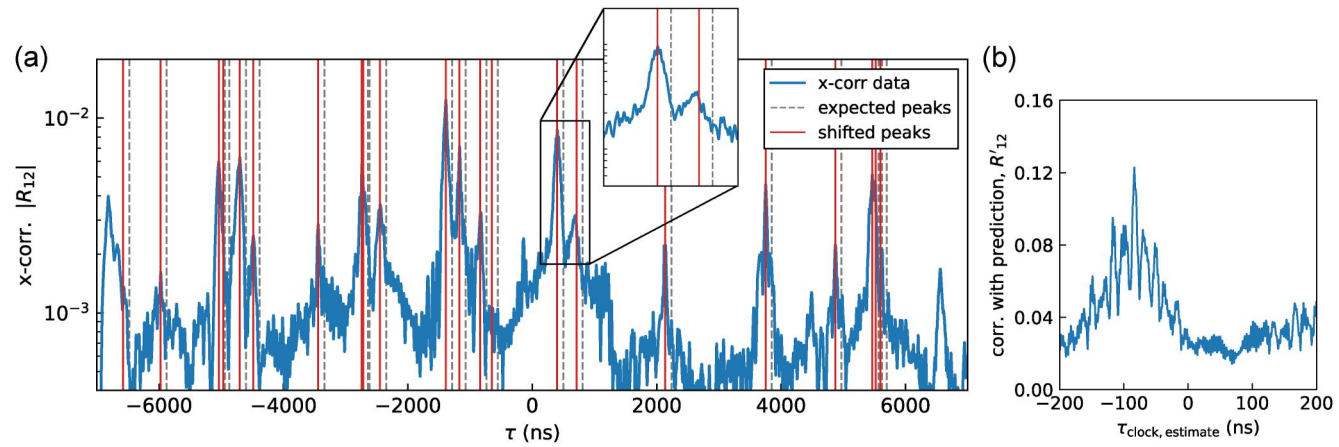

FIGURE 4 Cross-correlation of raw data. (a) Exemplary correlation signal (blue) with expected peak positions for a vanishing clock bias (dashed grey) and after being shifted by the estimated clock bias from panel (b) (red). For better visibility the data has been smoothed using a Gaussian with a standard deviation of 20 samples. (b) Correlation of the expected peak signal with the data. The clock bias is estimated as the position of the maximum.

If necessary, the temporal resolution could be somewhat improved by falling back to filtering only high bandwidth signals, for example, the E5 band (approx. 50 MHz). Other than that, we estimate the minimum feasible distance to be on the order of several hundred metres. On the other end of the scale, differences in relative Doppler shifts between satellites cause an eventual decorrelation with increasing baselines, likely causing significant degradation of performance beyond a few tens of kilometres.

4.2 | Code correlation

A more complex approach is correlation of the individual GNSS signal codes and comparison of discrete chip arrival times with expectations. As GNSS signals are designed for optimal correlation properties and orthogonality to all other signals and satellites, a code correlation is usually possible even if a direct correlation shows too low SNR, allowing for accurate clock delay estimation even in the presence of interference. Individually analysing multiple frequency bands per satellite improves outlier detection and is typically the more robust method in the presence of interference as well as having no lower baseline limit (the upper limit depends on the acceptable number of satellites in common view as well as the ability to compensate for environmental factors).

The correlation coefficient is calculated as in Equation (3) with an additional normalisation factor $1/\min(\text{length}(y), \text{length}(\text{code}))$ to account for different PRN code lengths. This allows to set a fixed detection threshold for all signals regardless of their length. For each signal, the data analysis routine

1. Applies appropriate band-pass filter (a typical bandwidth is 30 MHz) to data,
2. Generates GNSS codes and modulates them with carrier frequency (including predicted Doppler shifts) for all visible satellites transmitting that signal,
3. Computes the cross-correlation signals $R_{12}(\tau)$,
4. Obtains the envelope functions from absolute values of the Hilbert transforms,
5. Finds peak positions and calculates τ_{clock} from weighted TDoA averages per satellite.

Exemplary Galileo E5B correlation signals are shown in Figure 5 with clearly visible peaks at distances of 1 ms, as expected from the primary code repetition rate of 1 kHz. Peaks that appear in both signals and lie closer than for example, 1 µs after shifting by their expected TDoA (zoom panel) are evaluated as pairs in the clock offset computation.

The maximum-likelihood estimator of the clock bias τ_{clock} is an inverse-variance weighted arithmetic mean of individual delays. The relative code delays of an individual PRN signal are reduced to a mean value with uncertainty $\Delta\text{TDoA} = \sigma_{\text{TDoA}}/\sqrt{N-1}$ where N is the detected peak count and σ_{TDoA} is the standard deviation of the relative delay data sample. As an example, for the 50 peaks found in the shown signal over its

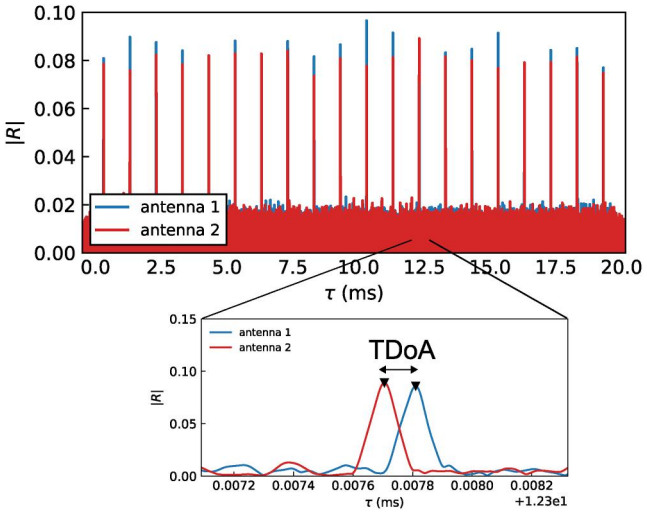

FIGURE 5 Exemplary correlation signal of band-pass filtered data with locally generated Galileo E5B pilot code. The bottom panel shows a close-up view of the indicated region to reveal the shape of a single correlation peak pair whose maxima are marked with black triangles.

full 50 ms duration, the standard error is $\Delta\text{TDoA} = 3.19\,\text{ns}/\sqrt{49} = 0.46\,\text{ns}$. All TDoA_i are corrected for their expected value, followed by the computation of the final average with weights of $(\Delta\text{TDoA}_i)^{-2}$; the remaining standard error of the clock offset τ_{clock} is $\sigma_\tau = \left(\sum_i (\Delta\text{TDoA}_i)^{-2}\right)^{-\frac{1}{2}}$. We found that setting an upper limit for individual weights (e.g. all signals with $\Delta\text{TDoA}_i < 1$ ns are weighted equally) significantly reduces the standard deviation of successive measurements as otherwise signals with unusually low ΔTDoA dominate the weighted average and hence reduce the multi-channel advantage of this method.

The reproducibility of results over repeated measurements are shown in Figure 6 for time series collected in both the single (Figure 6a) and independent ADC configurations both with and without the presence of a strong clock drift (Figure 6b,c). All datasets are shifted towards zero for better understanding.

For the single ADC measurement, all timing errors lie within a ±1 ns interval over the course of around 10 minutes and exhibit a standard deviation of 250 ps. The measurements continued at five-minute intervals over the course of 22 h, with the standard deviation of all points (not shown here) remaining unchanged and 95 % deviating by less than 660 ps from the mean. Additionally, no systematic diurnal bias was observed. The remaining statistically estimated single-point uncertainties σ_τ of individual data points after the averaging process are of order 100 ps. Despite having its strength in single record performance, averaging over for example, 5 minutes can reduce the synchronisation precision to around 30 ps under the assumption of perfect clock stability during the averaging time period.

For measurements carried out with separate ADCs and clocks, the data point spread is 460 ps during the measurement

period of 25 min for a stable running clock and, unsurprisingly, much larger for a perturbed clock, since changes in clock bias are directly reflected in the data. Indeed, the major contribution to the standard deviation seems to be a continuous drift occurring on timescales of minutes as offsets of successive data points are typically strongly correlated over that time, hence we attribute the data bias to be a drift of the caesium or rubidium clock. To separate this behaviour in the evaluation, we calculate a trend of the data using a 1/(120 s) low-pass filter. After subtraction of the trend, the standard deviation of the code correlation method drops to around 220 ps for the stable clock and 260 ps for the perturbed clock dataset, which is comparable to the uncertainties of individual points and nearly equal to the timing performance measured with a single ADC. The cross-correlation method performs slightly better with a remaining standard deviation w.r.t. its trend of approx. 200 ps in both cases. We find that the clock bias measurement of a commercial device is not able to resolve the slow relative clock drift as shown in Figure 6b. However, larger drifts as shown in panel c are fully resolved and confirm that the experimental data reproduces the clock drift. Small discrepancies w.r.t. the bias output of the single-antenna GNSS clock may be due to a drift of the caesium clock that is not monitored with sufficient accuracy during the measurement or an ordinary timing error of the device.

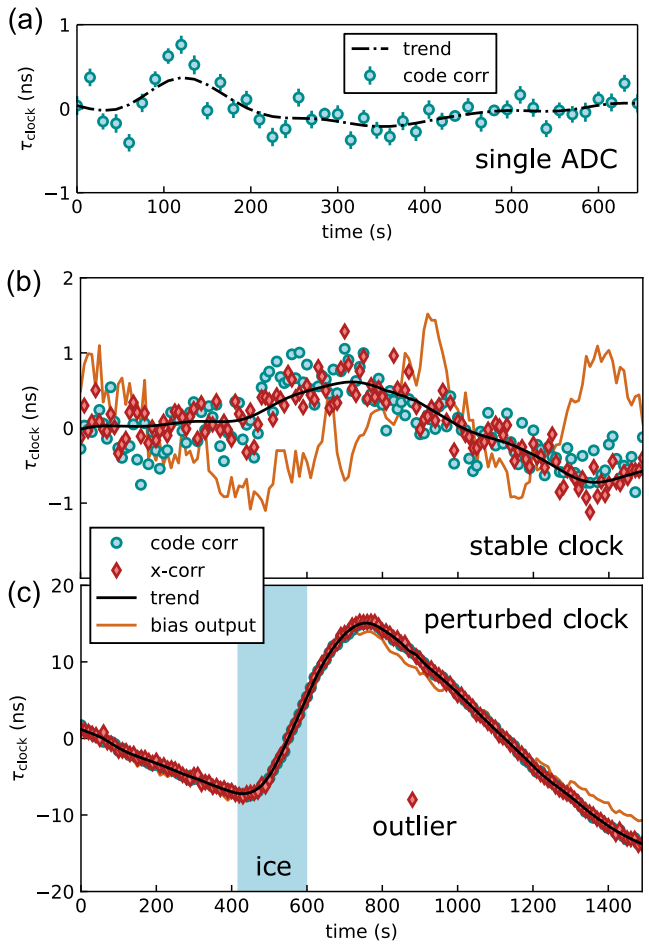

FIGURE 6 Evaluation of clock delay stability measurements. A global offset is subtracted in all plots for better understanding. (a) Results of code correlation with both antennas connected to a single ADC (short baseline) (b), (c) Results of both methods with separate ADCs and clocks (long baseline) for (b) stable clocks and (c) an experiment where the second site's rubidium clock was deliberately perturbed by a temperature drop caused by application of a cooling pack to the housing. Both datasets heavily overlap, hence only one can be seen properly. The shaded region represent the duration of the perturbation. In both (b) and (c), the bias of the rubidium clock relative to UTC estimated by a separate GNSS receiver is shown for comparison. Occasional outliers like the annotated point in panel (c) also appear in (b) but lie outside the plotting range.

5 | DISCUSSION

We find that both methods are capable of achieving a similar level of accuracy in good conditions, namely provided an acceptable number of visible satellites, absence of strong interference in GNSS bands, a baseline length within the constraints of the raw cross-correlation method and record lengths containing a high number of correlation peaks. Under these circumstances, raw cross-correlation has a clear advantage in both lower computation complexity. The change in precision for differing conditions can be estimated with the Cramèr-Rao lower bound of a TDoA estimation uncertainty which scales with $\sigma_{\mathrm{TDoA}} \propto 1/\sqrt{SNR}$ [6] (analogously to the standard error of the weighted average), where SNR is the signal-to-noise ratio, and can thus be expected to scale with the inverse square root of the record length, number of detected GNSS peaks and overall signal level. While experimental conditions have not been deliberately varied, an additional evaluation for truncated record lengths was made. Figure 7 shows that code correlation precision increases, as

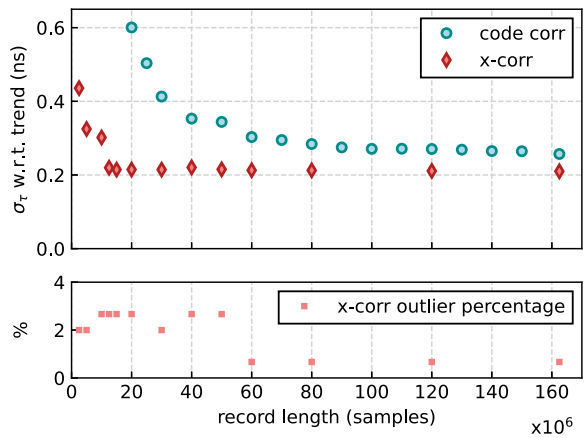

FIGURE 7 Impact of record length on the precision of both methods. Values of σ_τ were calculated for truncated records of the perturbed clock dataset shown in Figure 6c as the standard deviation of points with respect to the trend. The outlier percentage (out of a total of 150 records) arising in the cross-correlation method is shown in the bottom part of the plot. Code correlation did not yield outliers.

expected, by roughly the square root of the sample count. The cross-correlation method, however, is less affected by SNR issues and reaches its final performance already at a record length of around 20×10^6 samples but with occasional outliers. Considering that those values already lie significantly below our sample spacing of approx. 300 ps, a further precision improvement is hardly expected. On the other hand, the code correlation method does not suffer from baseline length limitations and is more robust given that it did not produce any outliers in our analysis.

Even though successive measurements often yield similar results, systematic drifts are visible in the data. As these drifts are present even in recordings gathered by the same ADC (Figure 6a), clock instabilities can be ruled out as their sole source. The dominant effects causing the drifts are likely to stem from imprecise knowledge of antenna positions and multipathing biases [16]. Applying the detrending correction described above to this data set, although likely not well matched to the characteristic time of these processes, results in a reduction of the standard deviation by some 20 %.

6 | CONCLUSIONS

With our presented method, relative biases of remote clocks can be determined with a single record precision of $\sigma_\tau <$ 300 ps, improving to around 30 ps when averaged over 5 minutes under the assumption of zero clock drift. The accuracy of the method could not yet be tested over longer baselines due to missing infrastructure but is planned in future work.

The code correlation method could be further enhanced by optimising the computation speed to decrease the time interval between measurements and by determining the navigation message bit and/or the overlay code shift register state in every chip, effectively increasing the *SNR*. As data signal components are typically transmitted with lower power than the pilot components and their inclusion would lead to an estimated gain of 10%–20 %, the immense computational overhead is not tenable at present. Moreover, outliers in the cross-correlation method could be caught beforehand with a procedure that automatically applies notch filters to interference signals.

AUTHOR CONTRIBUTIONS

Erik Busley: Conceptualisation; Formal analysis; Investigation; Software; Visualisation; Writing – original draft. **Timotej Žuntar:** Conceptualisation; Formal analysis; Investigation; Software; Visualisation; Writing – original draft. **Jörg Borgmann:** Conceptualisation; Project administration; Software; Supervision; Writing – review & editing. **Michael Krist:** Funding acquisition; Project administration; Resources; Supervision; Writing – review & editing.

ACKNOWLEDGEMENT

Open Access funding enabled and organized by Projekt DEAL.

CONFLICT OF INTEREST STATEMENT

The authors declare no potential conflict of interests.

DATA AVAILABILITY STATEMENT

The data that support the findings of this study are available from the corresponding author upon reasonable request.

REFERENCES

1. Beasley, P.J., et al., IET Radar: Sonar & Navigation (2023)
2. Sandenbergh, J.S., Inggs, M.R. In: IEEE Radar Conference (RadarConf), pp. 1640–1645 (2017)
3. Ali, B., Antoniou, M., Baker, C.J. In: IEEE Transactions on Geoscience and Remote Sensing, vol. 60, pp. 1 (2022)
4. Hoffmann, R., et al. In: IEEE Radar Conference (RadarConf), pp. 1–6 (2019)
5. 5. Petit, G., Thomas, C., Moussay, P., Davis, J., Miranian, M., Palacio, J., 11 (1997)
6. Peter, Jg.T., Oliver, M., Springer Handbook of Global Navigation Satellite Systems, vol. 10, (Springer2017)
7. Plank, L., et al.: VLBI observations of GNSS-satellites: from scheduling to analysis. J. Geodesy 91(7), 867–880 (2017). https://doi.org/10.1007/s00190-016-0992-8
8. State Ministry of the Interior of Northrhine-Westphalia . https://www.geoportal.nrw/
9. Interface Control Working Group: NAVSTAR GPS Space Segment/Navigation User Segment Interfaces. https://www.gps.gov/technical/icwg/IS-GPS-200N.pdf
10. Interface Control Working Group: NAVSTAR GPS Space Segment/User Segment L5 Interfaces. https://www.gps.gov/technical/icwg/IS-GPS-705J.pdf
11. European Union: European GNSS Open Service Signal-In-Space Interface Control Document. https://www.gsc-europa.eu/sites/default/files/sites/all/files/Galileo_OS_SIS_ICD_v2.0.pdf
12. China Satellite Navigation Office: BeiDou Navigation Satellite System Signal in Space Interface Control Document. http://en.beidou.gov.cn/SYSTEMS/Officialdocument/201902/P020190227601370045731.pdf
13. Kelso, T.S.: NORAD GP Element Sets. https://celestrak.org/NORAD/elements/
14. Rhodes, B.: Skyfield: High Precision Research-Grade Positions for Planets and Earth Satellites Generator, pp. 024. Astrophysics Source Code Library (2019). record ascl:1907
15. Harris, C.R., et al., Array programming with NumPy. Nature 585(7825), 357–362 (2020). https://doi.org/10.1038/s41586-020-2649-2
16. Levine, J.: Position, navigation, and timing technologies in the 21st century: integrated satellite navigation. Sensor Syst. Civil Applicat. 1, 821 (2020)

How to cite this article: Busley, E., et al.: Time transfer via single-record TDoA measurements of GNSS satellites using direct cross-correlation and relative pilot code phases. IET Radar Sonar Navig. 18(12), 2447–2453 (2024). https://doi.org/10.1049/rsn2.12557